

RSC Advances



This is an *Accepted Manuscript*, which has been through the Royal Society of Chemistry peer review process and has been accepted for publication.

Accepted Manuscripts are published online shortly after acceptance, before technical editing, formatting and proof reading. Using this free service, authors can make their results available to the community, in citable form, before we publish the edited article. This *Accepted Manuscript* will be replaced by the edited, formatted and paginated article as soon as this is available.

You can find more information about *Accepted Manuscripts* in the [Information for Authors](#).

Please note that technical editing may introduce minor changes to the text and/or graphics, which may alter content. The journal's standard [Terms & Conditions](#) and the [Ethical guidelines](#) still apply. In no event shall the Royal Society of Chemistry be held responsible for any errors or omissions in this *Accepted Manuscript* or any consequences arising from the use of any information it contains.



Journal Name

ARTICLE

Light absorption enhancement by embedding submicron scattering TiO₂ nanoparticles in perovskite solar cells†

Received 00th January 20xx,
Accepted 00th January 20xx

Jun Yin,^{ab} Hui Qu,^a Jing Cao,^b Huilin Tai,^c Jing Li,^{*ac} and Nanfeng Zheng,^{*b}

DOI: 10.1039/x0xx00000x

www.rsc.org/

Efficient light absorption is a key issue for hybrid perovskite solar cells (PSCs) to achieve better photovoltaic performances. Here, we introduce submicron scattering TiO₂ (s-TiO₂) nanoparticles into the mesoporous TiO₂ layer to improve the overall light harvesting efficiency in PSCs. Obviously enhanced current density and power conversion efficiency (PCE) were accomplished due to the improved light trapping in the active layer. Corresponding enhancement mechanisms were studied by the absorption spectra and finite-difference time-domain (FDTD) simulation results. Electrochemical impedance spectroscopy (EIS) measurements were further carried out to investigate the charge transportation process influenced by introducing s-TiO₂ into the mesostructure layer. With the optimized amount of embedded s-TiO₂, an average of over 5% PCE enhancement with an efficiency up to 16.72% was achieved comparing with the regular mesostructured PSCs.

Introduction

Efficient optical absorption by well-controlled light manipulation with reduced reflection or transmission loss is important in all types of solar cells for performance improvement and cost reduction, especially in thin-film solar cells.¹⁻⁴ Besides the mostly used anti-reflection films, various of light trapping nanostructures, such as graded-refractive-index materials,^{5, 6} plasmonic nanoparticles (NPs),^{7, 8} or dielectric nano-resonators,^{9, 10} have been introduced into thin-film solar cells for efficient light absorption enhancement by utilizing their unique light manipulation abilities, like anti-reflection, scattering or low-Q cavity resonance. Hybrid perovskite solar cells (PSCs), as a rising star in thin-film photovoltaic devices with superior advantages in power conversion and fabrication cost,¹¹ are also expected to achieve further photovoltaic performance improvement through the effective light manipulation. Recently, modified TiO₂ electron extraction layer,¹²⁻¹⁵ patterned FTO substrates,^{16, 17} metallic plasmonic NPs,¹⁸⁻²⁰ roughed interfaces²¹ or other functionalized nanostructures^{22, 23} have been employed or proposed to improve the light trapping in the PSC devices. Especially, as a widely used anode material with low cost, abundant synthesizable morphologies and reliable electron transport

property, nanostructured TiO₂ shows the promising light manipulation ability in PSCs, similar to that in the conventional DSSCs.²⁴

Here, we propose the embedding of submicron dielectric NPs into the mesoporous layer for absorption enhancement in PSCs by utilizing their scattering effects. The well-known commercial scattering TiO₂ (defined as "s-TiO₂") NPs in the typical size of ~160 nm (diameters ranged from 100 nm to 200 nm) were selected as an example of the scattering medium in the PSC structure. With s-TiO₂ embedded in mesoporous TiO₂ (named as "m-TiO₂") layer of perovskite film, the prominent light absorption enhancement and thus photovoltaic performance improvement were successfully achieved. The scattering phenomena and absorption enhancement were visually evidenced by the intensified near field and absorption profiles in FDTD simulation results. The effect of the embedded s-TiO₂ on the electron transportation and photovoltaic performances was also revealed by EIS measurements. With compromising of the light trapping effect and the accompanied charges transportation loss, a satisfied photovoltaic performance with exceeding 5% average PCE improvement comparing with the regular mesostructured PSCs was realized by employing the optimized amount of s-TiO₂ in the mesostructure layer.

Results and Discussion

In a conventional mesostructured PSC (such as with m-TiO₂) as illustrated in **Figure 1a**, most of the incident light travels through the perovskite film layer in a transmission mode and part of the light would loss due to the limited thickness of active layer, especially in the longer wavelength region with relative lower absorption coefficient.^{11, 25} When introducing scattering NPs (e.g. s-TiO₂) into the active layer, as illustrated

^a Collaborative Innovation Center for Optoelectronic Semiconductors and Efficient Devices, Pen-Tung Sah Institute of Micro-Nano Science and Technology, Xiamen University, Xiamen, 361005, China. E-mail: lijing@xmu.edu.cn

^b State Key Laboratory for Physical Chemistry of Solid Surfaces, Collaborative Innovation Center of Chemistry for Energy Materials, and Department of Chemistry, College of Chemistry and Chemical Engineering, Xiamen University, Xiamen 361005, China. E-mail: nfzheng@xmu.edu.cn

^c State Key Laboratory of Electronic Thin Films and Integrated Devices, University of Electronic Science and Technology of China, Chengdu, 610054, China.

† Electronic Supplementary Information (ESI) available: Experimental details and supplementary data. See DOI: 10.1039/x0xx00000x

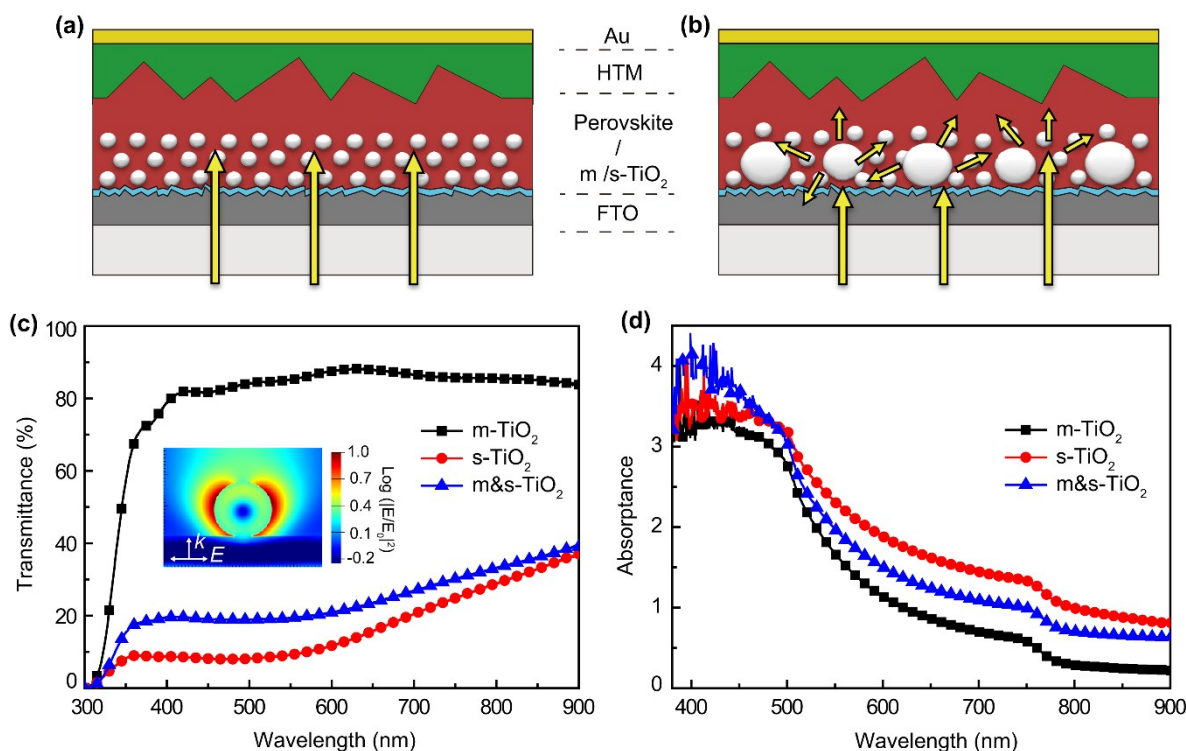


Figure 1. Schematic illustration of the light transmission mechanisms for (a) the regular mesostructured perovskite solar cells and (b) the s-TiO₂ NPs embedded perovskite solar cells. (c) Transmittance spectra of the m-TiO₂, s-TiO₂ and m&s-TiO₂ samples on FTO substrates. The obvious transmission decrement was originated from the scattering effect from the s-TiO₂ NPs, as demonstrated in the extracted near-field distribution pattern by FDTD simulation (inset). (d) Absorption spectra for the three types of mesostructured perovskite films with: m-TiO₂, s-TiO₂ and m&s-TiO₂, respectively.

in Figure 1b, the scattering effect would change the light from radiation mode to scattering mode,^{26, 27} which would facilitate the effective light absorption in the two-dimensional perovskite thin film. As a result, the short-circuit current density (J_{sc}) in PSCs can be expected to be increased as well as the overall PCE.

Evidently, as shown in Figure 1c, with comparison to the high transparency in the m-TiO₂ sample on FTO substrate, a distinguished transmittance decrement in the visible region was demonstrated in both scattering particles deposited FTO substrates, either in s-TiO₂ or s-TiO₂ embedded into m-TiO₂ (named as “m&s-TiO₂”) samples. The scattering effect in the layer containing s-TiO₂ NPs (in an average diameter of ~160 nm), mainly happened in the visible region, is believed to be responsible for the prominent light transmission reduction, as verified by the simulated extinction spectra (Figure S1a, ESI[†]) and extracted near-field distribution in inset of Figure 1c. Especially, the wide range of size distribution (100 to 200 nm) for s-TiO₂ and induced different scattering regions (Figure S1b) resulted in a broadband transmittance decrement. Because of the change of the external refractive index, the scattering effect in m&s-TiO₂ sample was slightly decreased when compared to the bare s-TiO₂ sample, as illustrated in the transmission spectra (Figure 1c). These transparency changes also can be visualized from the photographs of the samples shown in Figure S1c (ESI[†]), in which the only s-TiO₂ deposited FTO substrate shows the most blurriness. As expected, the

absorption enhancement can be realized on the perovskite films when employing scattering TiO₂ NPs into the active layer, as shown in Figure 1d. The light harvesting efficiency (LHE) calculated from the reflectance and absorbance spectra²⁸ indicates that the absorption enhancement mainly happened in the wavelength region from ~550 nm to 750 nm (Figure S2, ESI[†]).

In order to further demonstrate the influence of the scattering effect induced by the incorporation of submicron TiO₂ NPs on the performances of PSCs, s-TiO₂ NPs and s-TiO₂ embedded m-TiO₂ (m&s-TiO₂) mesostructures were used to fabricate the PSCs. The regular mesostructured devices were also fabricated as a reference for comparison. Here, the conventional solution-based two-step sequential method was firstly used to prepare the perovskite layer (see experimental details in the ESI[†]).²⁹ The SEM images of the device structure (Figure S3, ESI[†]) indicate that there is no significant differences in the film thickness among these samples except for relatively poorer film uniformity in the s-TiO₂ sample, which might be caused by the unsatisfied film-formation due to the incorporation of the submicron NPs in a rather larger size. However, the consequent spin coating of m-TiO₂ on the deposited s-TiO₂ film helped to improve the film uniformity (Figure S3f, ESI[†]). On the other hand, the as-prepared films using the three types of mesostructures exhibit no obvious differences in their perovskite’s crystallinity, as demonstrated by their XRD patterns (Figure S4, ESI[†]). The typical J - V curves

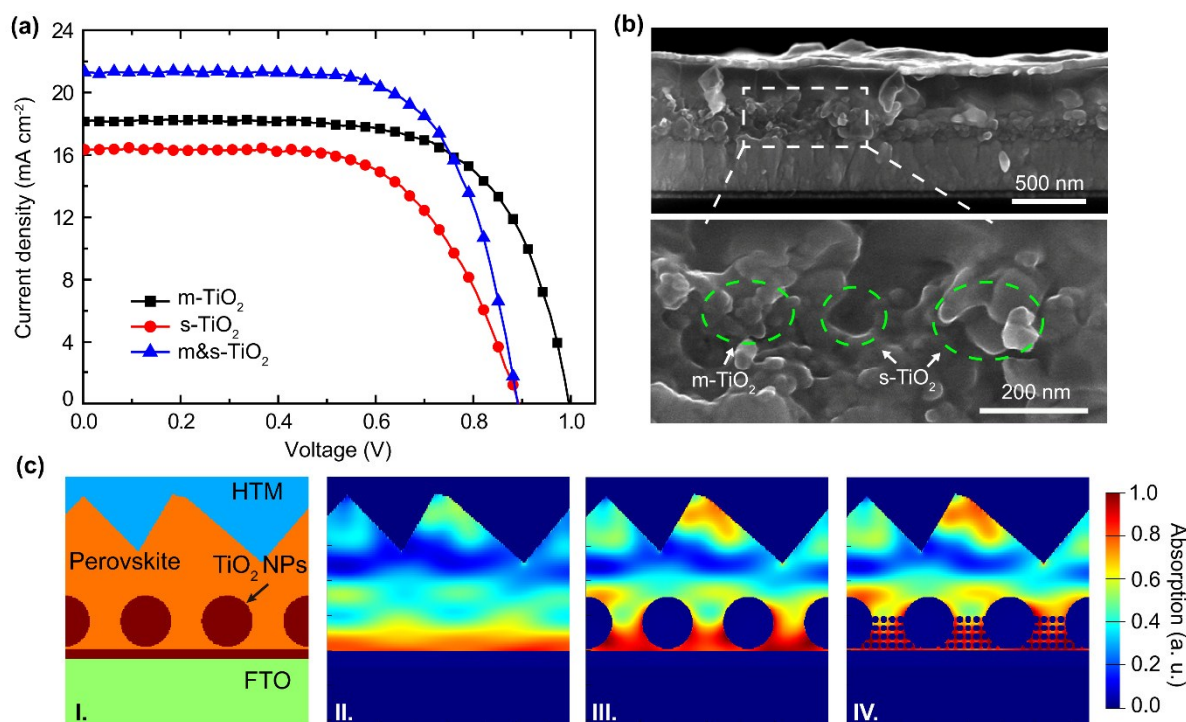


Figure 2. (a) J - V curves for the three types of mesostructured PSCs: m-TiO₂, s-TiO₂ and m&s-TiO₂, respectively. (b) Cross-sectional SEM image of the PSC device using m&s-TiO₂ as mesoporous layer; (c) The (I.) FDTD simulation model and (II-IV.) correspondingly simulated absorption profiles (at wavelength of 600 nm) for the m-TiO₂, s-TiO₂ and m&s-TiO₂, mesostructured PSCs, respectively. To simplify the simulation, the model consists of: perovskite layer about 320 nm-thick with rough surface, periodic spherical s-TiO₂ NPs (diameter of 160 nm) in a period of 240nm, and semi-limited HTM layer and FTO substrates. Periodic boundary conditions (PBC) has been applied in the two-dimensional plane in the simulations.

Table 1. Summarized device parameters of the three types of mesostructured PSCs that shown in Figure 2a

Cell	V_{oc} (V)	J_{sc} (mA cm ⁻²)	FF	PCE (%)	R_s (Ω cm ⁻²)
m-TiO ₂	1.00	18.14	0.67	12.10	6.02
s-TiO ₂	0.89	16.49	0.62	9.11	10.78
m&s-TiO ₂	0.89	21.22	0.68	12.95	5.65

and photovoltaic parameters in the devices with the three types of configurations are shown in **Figure 2a** and **Table 1**, respectively. When only s-TiO₂ NPs were used to fabricate the mesoporous layer, a lower J_{sc} and open-circuit voltage (V_{oc}) were obtained by comparing with the regular mesostructured ones (m-TiO₂). While if s-TiO₂ NPs were embedded into the mesoporous TiO₂ (m&s-TiO₂), an obvious J_{sc} and PCE increments were realized although a lowered V_{oc} was still observed. As clearly shown in Figure 2b, the s-TiO₂ NPs embedded in the m-TiO₂ and perovskite bilayer can be well resolved. Undoubtedly, the obvious J_{sc} improvement for the m&s-TiO₂ sample should be originated from the enhanced light absorption efficiency (Figure 1d). The scattering effect of submicron TiO₂ NPs could be the main factor for the enhanced light absorption in the devices. As for the only s-TiO₂ sample, in spite of the enhanced absorption when comparing with both the regular m-TiO₂ and m&s-TiO₂ structures, much lower J_{sc} ,

V_{oc} and PCE were obtained. The poorer electron transportation ability of the films containing only submicron scattering NPs should be the responsible factor for the performance retardation, which will be discussed later in more details.

Base on the FDTD simulation model (Figure 2c-I) and referenced dielectric permittivity of CH₃NH₃PbI₃ and HTM materials from the early reports,³⁰⁻³² absorption profiles in the three different types of mesostructured PSCs were calculated to verify the absorption enhancement mechanism. Comparing to the absorption profile for the only perovskite layer in Figure 2c-II, much stronger absorption can be visualized near the s-TiO₂ NPs (Figure 2c-III), which undoubtedly was induced by the scattering effect. Understandably, enhanced absorption (Figure 2c-IV) can also be obtained in the m&s-TiO₂ mesostructured PSC.

However, it should be noted that the V_{oc} decrement after introducing s-TiO₂ would definitely limit the further improvement of PCE. We therefore carried out electrochemical impedance spectroscopy (EIS) measurements (**Figure 3**) to evaluate the charge transportation resistance (R_{ct}) for different-structured devices. Obviously, the main arcs shown in Figure 3a are attributed to charges extraction between the perovskite and TiO₂ electron transport layer (ETL),^{33, 34} which correspond to the combination of the charge-transfer-resistance (R_{ct}) and the chemical capacitance (C_{μ}) of the film. The EIS spectra can be well fitted using the equivalent circuit model³⁵ and R_{ct} was extracted and plotted as a function

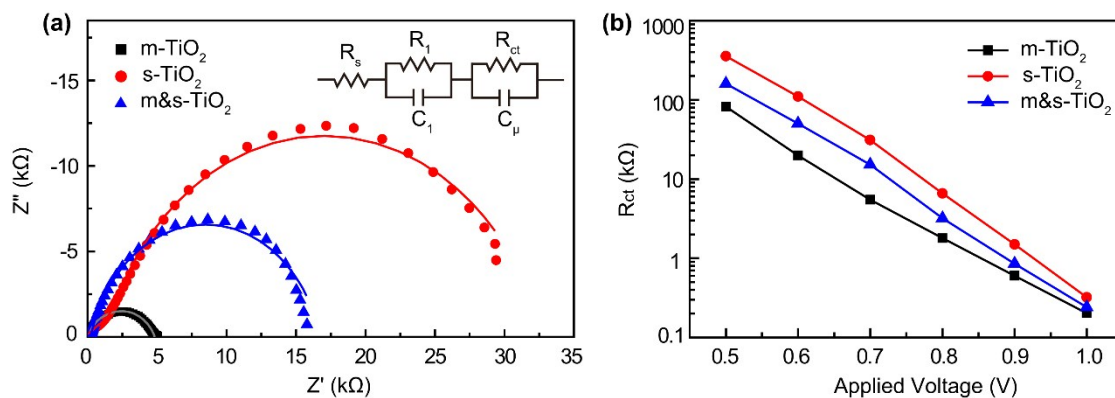


Figure 3. (a) Nyquist plots and corresponding fitted curves (solid lines) for the three type of mesostructured PSCs: m-TiO₂, s-TiO₂ and m&s-TiO₂ (bias voltage was 0.7 V). The measurement was taken under dark condition and the equivalent circuit employed to fit the spectra was shown in inset. R_s is the series resistance; R₁ and C₁ represent the hole transport resistance and capacitance through the hole transport material (HTM) layer. (b) The extracted R_{ct} as a function of the applied voltage bias in the three samples.

of the applied voltage bias (Figure 3b). In comparison with the regular m-TiO₂ configured PSC devices, enlarged R_{ct} over the whole range of the applied voltages was characterized in both s-TiO₂ and m&s-TiO₂ mesostructured PSCs, indicating the retarded charge transportation process. Different from the

suppression of electron recombination with increased recombination resistance (R_{rec}),^{36, 37} the enlarged R_{ct} due to the declined charge transportation process should have no help to the V_{oc} and FF improvement. In contrast, the large R_{ct} would induce a severe decreased PV performance.^{33, 38} Generally,

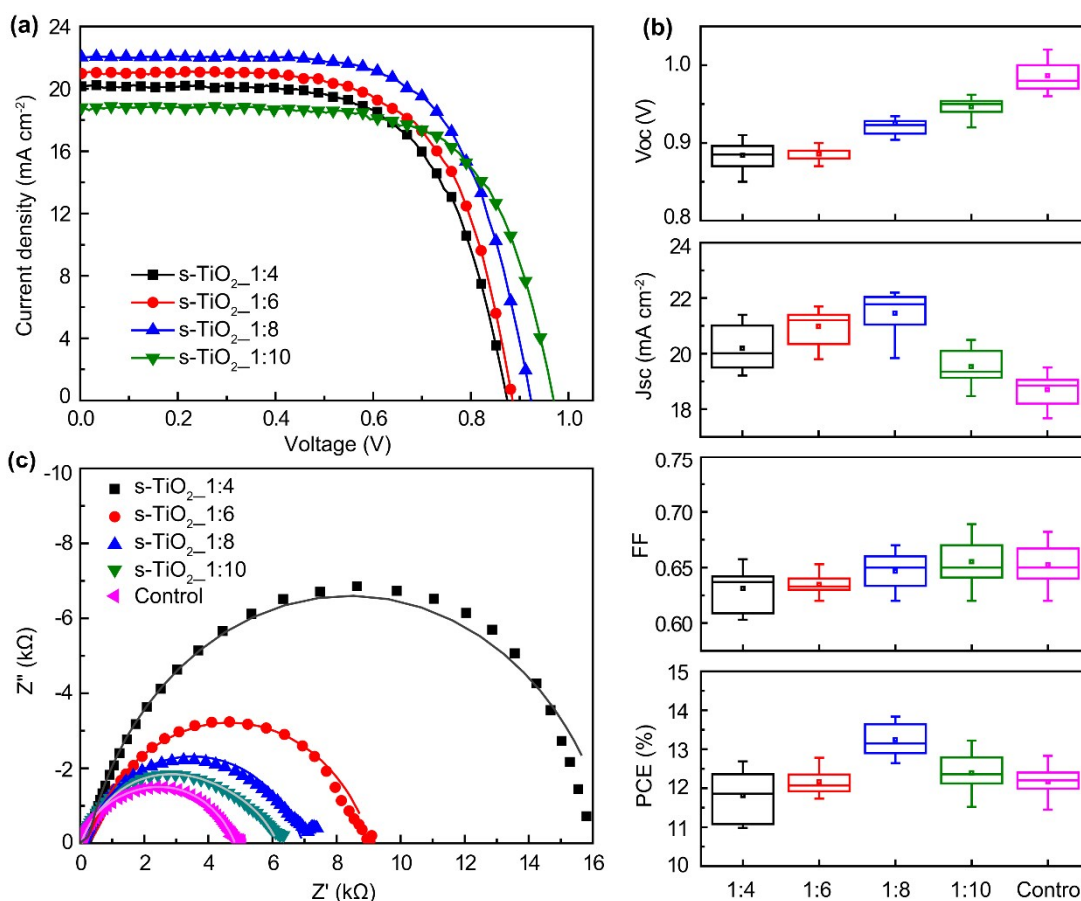


Figure 4. (a) *J-V* curves for the m&s-TiO₂ mesostructured PSCs with different amount of s-TiO₂ NPs by changing the dilution ratio of s-TiO₂ paste: 1:4, 1:6, 1:8, and 1:10, respectively. (b) Summarized photovoltaic parameters that extracted from the *J-V* measurements for the series of m&s-TiO₂ mesostructured PSCs as in (a). (c) Nyquist plots and fitted curves (solid lines) for the series of m&s-TiO₂ mesostructured PSCs as in (a). The control devices of the regular m-TiO₂ mesostructured PSCs were characterized also as a comparison.

poor surface condition (surface states) and inter-connection always present on the submicron s-TiO₂ NPs, which would not only limit the charge's effective transportation between perovskite and TiO₂ layer, but also lower the electron density in conduction band of TiO₂,³⁹ and thus induce the band edge shift (or quasi Fermi level) in TiO₂ photoanode.⁴⁰ Consequently, a reduced V_{oc} in TiO₂ photoanode based solar cells accompanied with a decrement in J_{sc} would happen. As a result, in the only s-TiO₂ mesostructured PSC device, the poorer photovoltaic performance was obtained (Figure 3a). In comparison, besides the scattering effect from s-TiO₂ NPs, the well-maintained charge transportation channels through the m-TiO₂ NPs with relative high conductivity would also help to realize an obvious J_{sc} increment in the m&s-TiO₂ mesostructured PSCs. However, the retarded charge transportation process still exists. Therefore, the amount of the embedded s-TiO₂ nanoparticles needs to be further optimized to achieve a satisfied PCE improvement.

Here, solutions with different concentrations were used to control the amount of s-TiO₂ in the mesostructure layer of perovskite film. The corresponding typical J - V curves are shown in Figure 4a with the summarized evolution of photovoltaic performances as a function of s-TiO₂ concentration shown in Figure 4b. It can be found that as the concentration of s-TiO₂ solution decreased a continuous V_{oc} increment happened in the corresponding devices with the

value more and more close to that in the regular m-TiO₂ mesostructured sample. Consistent with the above discussion and further evidenced by the EIS measurement (Figure 4c), the improved charges transportation (reduced R_{ct}) and subsequently increased electron density in conduction band of TiO₂ layer are responsible for this V_{oc} increment and corresponding FF improvement. Furthermore, as the amount of s-TiO₂ decreased, the reduced R_{ct} also facilitates the electron extraction in mesostructure layer, so that a further J_{sc} increment was obtained. However, as the concentration of s-TiO₂ continually dropped down to the dilution ratio of 1:10, the scattering based light trapping improvement becomes less prominent resulting in a relative lower J_{sc} , but which is still comparable to the value in regular mesostructured PSCs. According to the above demonstration, the best performance was obtained on the m&s-TiO₂ mesostructured PSCs with s-TiO₂ dilution ratio of 1:8. An average PCE of 13.25% (best of 13.84%) has been accomplished with a ~9% PCE improvement when compared with the regular mesostructured samples (12.17% in average).

Furthermore, by employing the newly developed solvent-assisted perovskite film preparation method (Experimental details, ES†),⁴¹ the photovoltaic performance for the m&s-TiO₂ mesostructured PSCs can be further improved to an average PCE of 16.01% (best of 16.72%), as shown in Figure 5a-b and Table 2. It still exhibit an obvious improvement (~5%) when

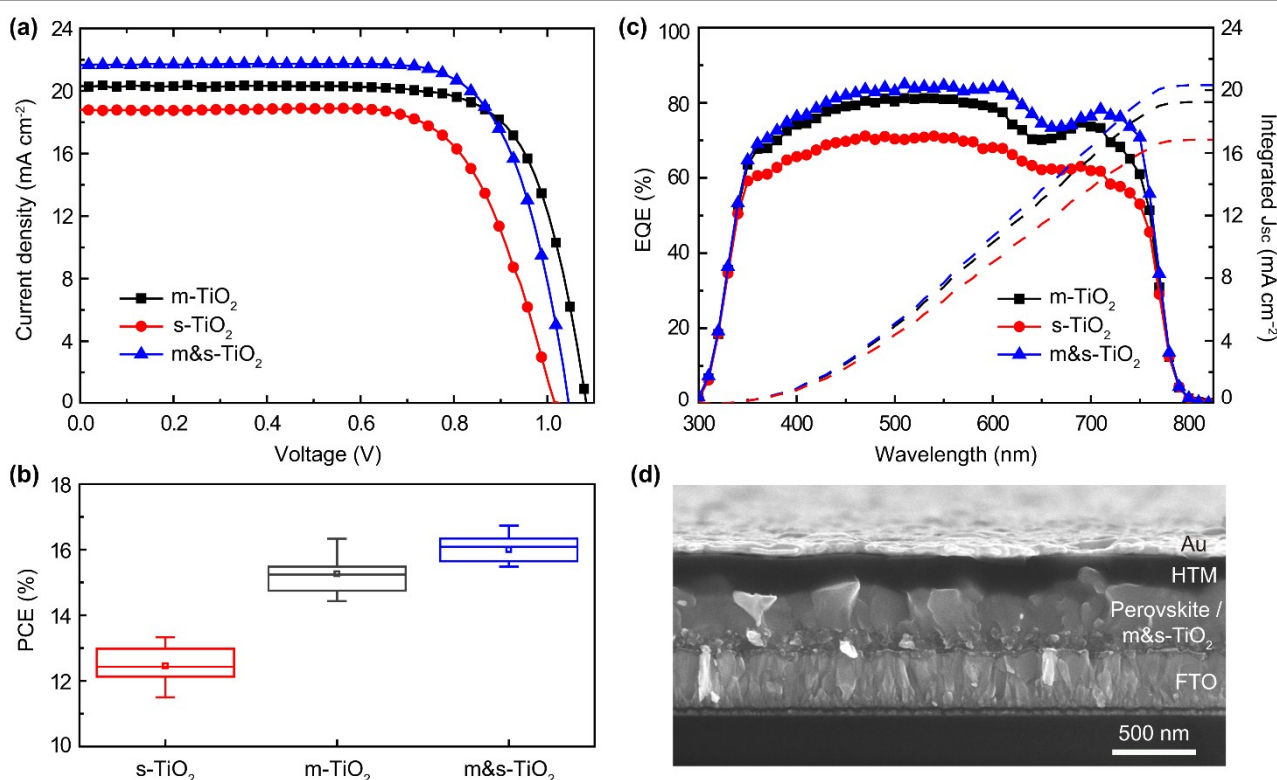


Figure 5. (a) J - V curves of the best performing cells for the three type of mesostructured PSCs, m-TiO₂, s-TiO₂ and m&s-TiO₂, using the solvent-assisted perovskite film preparation method. (b) Summarized PCE values for the prepared PSCs. (c) External quantum efficiency (EQE) spectra and corresponding integrated photocurrent density J_{sc} (dash lines) for the samples in (a). (d) Cross-section SEM image of the device with m&s-TiO₂ mesostructure layer using the solvent-assisted preparation method. Here, the optimized amount of s-TiO₂ in m&s-TiO₂ layer was used with the devices.

Table 2. Summarized device parameters of the best performing cells for the three type of mesostructured PSCs, m-TiO₂, s-TiO₂ and m&s-TiO₂, using the solvent-assisted perovskite film preparation method

Cell	V _{oc} (V)	J _{sc} (mA cm ⁻²)	FF	PCE (%)	R _s (Ω cm ⁻²)
m-TiO ₂	1.08	20.28	0.67	16.31	6.58
s-TiO ₂	1.02	18.77	0.62	13.33	9.54
m&s-TiO ₂	1.05	21.61	0.68	16.72	5.25

comparing with either the regular m-TiO₂ mesostructured samples (average PCE of 15.24%, best of 16.31%) or the only s-TiO₂ mesostructured samples (average of 12.46%, best of 13.33%). The integrated J_{sc} values based on external quantum efficiency (EQE) spectra (Figure 5c) were 19.24, 16.85, and 20.32 mA cm⁻² for the m-TiO₂, s-TiO₂ and m&s-TiO₂ samples shown in Figure 5a, respectively, and the results agree well with the J-V measurement values (Table 2). Certainly, the further enhanced photovoltaic performance is ascribed to the improved interface (Figure 5d) and crystallinity in the perovskite layer with a comparison to the samples prepared by the conventional two-step method (Figure S5, ESI[†]). In addition, the prepared champion cells are competitive to the current best-performed solution based PSCs that fabricated in open air with high humidity (≥ 40%).^{42, 43} The prepared PSCs also exhibit a satisfying hysteresis-less performance and light stability (Figure S6).

Conclusions

In conclusion, we have proposed a new strategy for light absorption improvement in perovskite based solar cells (PSCs) by utilizing the scattering effect of submicron dielectric nanoparticles (NPs). As an example, by introducing the submicron scattering TiO₂ (s-TiO₂) NPs into the mesostructure layer of perovskite film, an obviously increased J_{sc} was realized. The corresponding light trapping enhancement mechanisms were investigated through the absorption spectra and FDTD simulation. According to the J-V curves and EIS measurements, a better PCE improvement was predicted, which can be achieved through compromising the charges transportation loss and scattering based light absorption enhancement by optimizing the proportion of s-TiO₂ in mesoporous layer. In this manner, a PCE improvement by an average of over 5% was accomplished by employing optimized amount of s-TiO₂ in the PSCs when compared with the regular mesostructured cells.

This work well demonstrated a low-cost and good compatibility method to improve the light trapping and thus conversion efficiency in perovskite solar cells by introducing the Mie scattering dielectric NPs. The scattering medium proposed in this work also can be extended to other metallic plasmonic NPs or dielectric nanostructures to accomplish effective light management for efficient perovskite solar cells. Additionally, further photovoltaic performance improvement can be possibly achieved by eliminating the charges

transportation loss or additional recombination defects induced by these scattering nanostructures. So, further works, e.g. surface passivation, are worthy to be carried on.

Acknowledgements

This work is financially supported by the National Natural Science Foundation of China (Grant No. 61505172), China Postdoctoral Science Foundation Funded Project (No. 2015M582038), and the Open Foundation of State Key Laboratory of Electronic Thin Films and Integrated Devices (KFJJ201413).

Notes and references

‡ Footnotes relating to the main text should appear here. These might include comments relevant to but not central to the matter under discussion, limited experimental and spectral data, and crystallographic data.

§
§§
etc.

1. F. J. Haug and C. Ballif, *Energy Environ. Sci.*, 2015, **8**, 824-837.
2. A. Polman and H. A. Atwater, *Nature Mater.*, 2012, **11**, 174-177.
3. J. Zhu, C.-M. Hsu, Z. Yu, S. Fan and Y. Cui, *Nano Lett.*, 2010, **10**, 1979-1984.
4. J. Zhu and Y. Cui, *Nature Mater.*, 2010, **9**, 183-184.
5. J. Q. Xi, M. F. Schubert, J. K. Kim, E. F. Schubert, M. Chen, S.-Y. Lin, Liu W and J. A. Smart, *Nature Photon.*, 2007, **1**, 176-179.
6. C. Battaglia, J. Escarré, K. Söderström, M. Charrière, M. Despeisse, F.-J. Haug and C. Ballif, *Nature Photon.*, 2011, **5**, 535-538.
7. S. Carretero-Palacios, M. E. Calvo and H. Míguez, *J. Phys. Chem. C*, 2015, **119**, 18635-18640.
8. K. Catchpole and A. Polman, *Opt. Express*, 2008, **16**, 21793-21800.
9. G. Kang, J. Yoo, J. Ahn and K. Kim, *Nano Today*, 2015, **10**, 22-47.
10. J. Yin, Y. Zang, C. Yue, X. He, J. Li, Z. Wu and Y. Fang, *Phys. Chem. Chem. Phys.*, 2013, **15**, 16874-16882.
11. M. A. Green, A. Ho-Baillie and H. J. Snaith, *Nature Photon.*, 2014, **8**, 506-514.
12. H. Zhu, Y. Fu, F. Meng, X. Wu, Z. Gong, Q. Ding, M. V. Gustafsson, M. T. Trinh, S. Jin and X. Y. Zhu, *Nature Mater.*, 2015, **14**, 636-642.
13. H. Sun, P. Ruan, Z. Bao, L. Chen and X. Zhou, *Solid State Sci.*, 2015, **40**, 60-66.
14. Y. Yu, J. Li, D. Geng, J. Wang, L. Zhang, T. L. Andrew, M. S. Arnold and X. Wang, *ACS nano*, 2015, **9**, 564-572.
15. W. Q. Wu, F. Z. Huang, D. H. Chen, Y. B. Cheng and R. A. Caruso, *Adv. Funct. Mater.*, 2015, **25**, 3264-3272.
16. S. M. Kang, N. Ahn, J.-W. Lee, M. Choi and N.-G. Park, *J. Mater. Chem. A*, 2014, **2**, 20017-20021.
17. M. M. Tavakoli, K.-H. Tsui, Q. Zhang, J. He, Y. Yao, D. Li and Z. Fan, *ACS nano*, 2015, **9**, 10287-10295.
18. Z. Wang, J. Cui, J. Li, K. Cao, S. Yuan, Y. Cheng and M. Wang, *Mat. Sci. and Eng. B*, 2015, **199**, 1-8.
19. Z. Lu, X. Pan, Y. Ma, Y. Li, L. Zheng, D. Zhang, Q. Xu, Z. Chen, S. Wang, B. Qu, F. Liu, Y. Huang, L. Xiao and Q. Gong, *RSC Adv.*, 2015, **5**, 11175-11179.

20. S. S. Mali, C. S. Shim, H. Kim, P. S. Patil and C. K. Hong, *Nanoscale*, 2016, **8**, 2664-2677.
21. L. Zheng, Y. Ma, S. Chu, S. Wang, B. Qu, L. Xiao, Z. Chen, Q. Gong, Z. Wu and X. Hou, *Nanoscale*, 2014, **6**, 8171-8176.
22. B. W. Schneider, N. N. Lal, S. Baker-Finch and T. P. White, *Opt. Express*, 2014, **22**, A1422-A1430.
23. S. H. Hwang, J. Roh, J. Lee, J. Ryu, J. Yun and J. Jang, *J. Mater. Chem. A*, 2014, **2**, 16429-16433.
24. Y. Bai, I. Mora-Sero, F. De Angelis, J. Bisquert and P. Wang, *Chem. Rev.*, 2014, **114**, 10095-10130.
25. S. Sun, T. Salim, N. Mathews, M. Duchamp, C. Boothroyd, G. Xing, T. C. Sum and Y. M. Lam, *Energy Environ. Sci.*, 2014, **7**, 399-407.
26. H. J. Koo, Y. J. Kim, Y. H. Lee, W. I. Lee, K. Kim and N. G. Park, *Adv. Mater.*, 2008, **20**, 195-199.
27. F. Huang, D. Chen, X. L. Zhang, R. A. Caruso and Y. B. Cheng, *Adv. Funct. Mater.*, 2010, **20**, 1301-1305.
28. D. Y. Son, K. H. Bae, H. S. Kim and N. G. Park, *J. Phys. Chem. C*, 2015, **119**, 10321-10328.
29. J. Burschka, N. Pellet, S. J. Moon, R. Humphry-Baker, P. Gao, M. K. Nazeeruddin and M. Grätzel, *Nature*, 2013, **499**, 316-319.
30. P. Löper, M. Stuckelberger, B. Niesen, J. Werner, M. Filipič, S.-J. Moon, J.-H. Yum, M. Topič, S. De Wolf and C. Ballif, *J. Phys. Chem. Lett.*, 2014.
31. M. Filipič, P. Löper, B. Niesen, S. De Wolf, J. Krč, C. Ballif and M. Topič, *Opt. Express*, 2015, **23**, A263-A278.
32. G. Xing, N. Mathews, S. S. Lim, N. Yantara, X. Liu, D. Sabba, M. Grätzel, S. Mhaisalkar and T. C. Sum, *Nature Mater.*, 2014, **13**, 476-480.
33. H. S. Kim, I. Mora-Sero, V. Gonzalez-Pedro, F. Fabregat-Santiago, E. J. Juarez-Perez, N. G. Park and J. Bisquert, *Nature Commun.*, 2013, **4**, 2242.
34. H. S. Kim, J. W. Lee, N. Yantara, P. P. Boix, S. A. Kulkarni, S. Mhaisalkar, M. Grätzel and N. G. Park, *Nano Lett.*, 2013, **13**, 2412-2417.
35. J. Bisquert, *J. Phys. Chem. B*, 2002, **106**, 325-333.
36. J. Yin, J. Cao, X. He, S. F. Yuan, S. B. Sun, J. Li, N. F. Zheng and L. W. Lin, *J. Mater. Chem. A*, 2015, **3**, 16860-16866.
37. A. K. Chandiran, A. Yella, M. T. Mayer, P. Gao, M. K. Nazeeruddin and M. Grätzel, *Adv Mater*, 2014, **26**, 4309-4312.
38. Y. Yang, J. Xiao, H. Wei, L. Zhu, D. Li, Y. Luo, H. Wu and Q. Meng, *RSC Adv.*, 2014, **4**, 52825-52830.
39. G. Schlichthörl, S. Huang, J. Sprague and A. Frank, *J. Phys. Chem. B*, 1997, **101**, 8141-8155.
40. M. Wang, P. Chen, R. Humphry - Baker, S. M. Zakeeruddin and M. Grätzel, *ChemPhysChem*, 2009, **10**, 290-299.
41. W. S. Yang, J. H. Noh, N. J. Jeon, Y. C. Kim, S. Ryu, J. Seo and S. I. Seok, *Science*, 2015, aaa9272.
42. H.-S. Ko, J.-W. Lee and N.-G. Park, *J. Mater. Chem. A*, 2015, **3**, 8808-8815.
43. B. Lei, V. O. Eze and T. Mori, *Jpn. J. Appl. Phys.*, 2015, **54**, 100305.

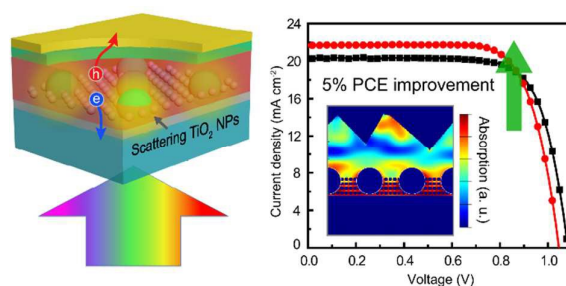
Graphical Abstract for:

Light absorption enhancement by embedding submicron scattering TiO₂ nanoparticles in perovskite solar cells

Jun Yin,^{ab} Hui Qu,^a Jing Cao,^b Huilin Tai,^c Jing Li,^{*ac} and Nanfeng Zheng,^{*b}

Efficient light absorption is a key issue for hybrid perovskite solar cells (PSCs) to achieve better photovoltaic performances. Here, we introduce submicron scattering TiO₂ (s-TiO₂) nanoparticles into the mesoporous TiO₂ layer to improve the overall light harvesting efficiency in PSCs. Obviously enhanced current density and power conversion efficiency (PCE) were accomplished due to the improved light trapping in the active layer. Corresponding enhancement mechanisms were studied by the absorption spectra and finite-difference time-domain (FDTD) simulation results. Electrochemical impedance spectroscopy (EIS) measurements were further carried out to investigate the charge transportation process influenced by introducing s-TiO₂ into the mesostructure layer. With the optimized amount of embedded s-TiO₂, an average of over 5% PCE enhancement with an efficiency up to 16.72% was achieved comparing with the regular mesostructured PSCs.

Table of contents Figure:



Scattering effect enhanced light absorption in perovskite solar cells (PSCs) from the embedded submicron dielectric nanoparticles (NPs) is demonstrated. With optimized amount of the embedded scattering NPs, obvious J_{sc} increment and consequent PCE improvement over 5% can be accomplished when comparing with the regular mesostructured PSCs.